Micro/nano-structure Co_3O_4 as high capacity anode materials for lithium-ion batteries and the effect of the void volume on electrochemical performance

CrossMark

Bin Zhang [a,b,c], Yibo Zhang [a,b], Zhenzhen Miao [a,b,c], Tianxiao Wu [a,b,c], Zhendong Zhang [a,b], Xiangguang Yang [a,b,*]

[a] State Key Laboratory of Rare Earth Resource Utilization, Changchun Institute of Applied Chemistry, Chinese Academy of Sciences, 5625 Renmin Street, Changchun 130022, PR China
[b] Laboratory of Green Chemistry and Process, Changchun Institute of Applied Chemistry, Chinese Academy of Sciences, 5625 Renmin Street, Changchun 130022, PR China
[c] Graduate University of Chinese Academy of Sciences, Beijing 100049, PR China

HIGHLIGHTS

- Facile method to prepare Co_3O_4 spheres and cubes with micro/nano-structure.
- The two Co_3O_4 materials are crystalline and uniform in morphology.
- The electrodes show superior cycling stability and excellent rate performance.
- The void volume is important to the electrochemical performance.

ARTICLE INFO

ABSTRACT

Two kinds of Co_3O_4 samples with micro/nano-structure as high capacity anode materials for Lithium-ion Batteries are synthesized by a facile method. The structure, composition and surface morphology are analyzed by means of X-ray diffraction (XRD), scanning electron microscopy (SEM) and high-resolution transmission electron microscopy (HRTEM), respectively. The XRD data indicates that the two Co_3O_4 materials are crystalline, single-phase without any impurity phase; the size of spheres and cubes are estimated to be 2 μm and the nanoparticles are around 100 nm. The cyclic voltammetry and discharge/charge measurements are carried out to detect the electrochemical properties. The results demonstrate that the two Co_3O_4 electrodes with micro/nano-structure exhibit low initial irreversible capacity and superior cycling performance. The two Co_3O_4 materials with micro/nano-structure are confirmed to combine the advantages of the micro-materials and nano-materials for LIBs. Moreover, the Co_3O_4 spheres (s-Co_3O_4) exhibit more superior cycling performance than that of Co_3O_4 cubes (c-Co_3O_4) due to the larger void volume in spheres than that in cubes structure.

1. Introduction

New power source with green technologies is urgently demanded due to consumption of fossil fuel. For this reason, chemical energy storage using rechargeable lithium-ion batteries (LIBs) has been becoming increasingly important for friendly environment [1,2]. So far, various materials, such as graphitic/non-graphitic carbon, transition-metal oxides (SnO_2, TiO_2, Fe_2O_3, Co_3O_4, MnO_2, MoO_3), chalcogenides (TiS_2), nitrides, polymers, lithium alloys (Si, Sn, Al, Sb)/multinary alloys, and their composites, have been exploited as the anode materials of LIBs [3—10]. Among them, Co_3O_4 has been given special attention owing to its high theoretical capacity (890 mAh g^{-1}), which is almost two and a half times of the graphite anode (372 mAh g^{-1}) [7].

For nanomaterials, the reduced dimension increases the rate of lithium insertion/removal and the electron transport significantly, because of the short distances for lithium-ion and electron transport within the particles. Plus, a high surface area permits a high contact area with the electrolyte and hence a high lithium-ion flux

* Corresponding author. Laboratory of Green Chemistry and Process, Changchun Institute of Applied Chemistry, Chinese Academy of Sciences, 5625 Renmin Street, Changchun 130022, PR China. Tel.: +86 431 85262228; fax: +86 431 85262687.
E-mail address: xgyang@ciac.ac.cn (X. Yang).

across the interface [11]. However, there are some disadvantages of nanomaterials for LIBs, e.g.: 1) high electrode surface area may lead to more significant side reactions with the electrolyte, and more difficulty maintaining interparticle contact, which results in the poor cyclic performance [12]; 2) the density of a nanopowder is generally less than the same material formed from micrometer-sized particles, the volume of the electrode increases for the same mass of material thus reducing the volumetric energy density [13]. The micrometer-sized materials can overcome the disadvantages as mentioned above, but the long Li ion diffusion path may result in a poor rate capability.

From this point of view, a micro/nano-structure is expected to provide a step forward by assuring excellent cyclic performance combined with excellent rate capability. In this paper, we report the facile synthesis of Co_3O_4 spheres and cubes morphology with micro/nano-structure, which are characterized by XRD and SEM measurements. The electrochemical analysis shows that the two Co_3O_4 electrodes exhibit low initial irreversible capacities, high capacities at different densities and superior cycling performance. We find that the micro/nano-structure plays important roles in improving the electrochemical performance of the electrodes for LIBs.

2. Experimental

2.1. Chemicals

All the chemical reagents purchased from Aladdin Chemical Reagent Corporation were analytical grade (AR) and used without further purification.

2.2. Synthesis of Co_3O_4 materials

Two kinds of Co_3O_4 materials with micro/nano-structure were synthesized via a facile route. Typically, $Co(NO_3)_2 \cdot 6H_2O$ and NH_4HCO_3 were dissolved in 60 mL of ethylene glycol. The mixture solution was stirred for 30 min and then transferred into a 100 mL of Teflon-lined autoclave. The mixed reactants were heated at 185 °C for 20 h and then cooled down to room temperature. The obtained pink products were washed with distilled water and ethanol for several times, and dried under vacuum at 60 °C for 10 h. And then the two kinds of products were calcined at 500 °C for 5 h. To prepare the s-Co_3O_4, the amounts of $Co(NO_3)_2 \cdot 6H_2O$ and NH_4HCO_3 were 1 g and 4 g, respectively; for the c-Co_3O_4, the amounts of $Co(NO_3)_2 \cdot 6H_2O$ and NH_4HCO_3 were 0.5 g and 4 g, respectively.

2.3. Structure characterization of Co_3O_4

The powder X-ray diffraction (XRD) patterns were carried out on a Bruker D8 Advance X-ray diffractometer using a Cu Kα radiation source (λ = 1.5406 Å). Scanning electron microscopy (SEM) was performed on a field emission Hetachi S-4800 instrument. Transmission electron microscopy (TEM) was performed using a FEI Tecnai G2 S-Twin instrument with a field emission gun operating at 200 kV. Nitrogen adsorption and desorption isotherms at 77.3 K were characterized on Micromeritics ASAP 2020. Mercury Porosimetry was characterized on AutoPore IV 9500 V1.09.

2.4. Electrochemical measurements

Co_3O_4 (70 wt%), Acetylene Black (AB, 15 wt%) and poly(-vinylidene fluoride) (PVDF, 15 wt%) were mixed with *N*-methyl-pyrrolidone, grounding with mortar and pestle for 30 min. The
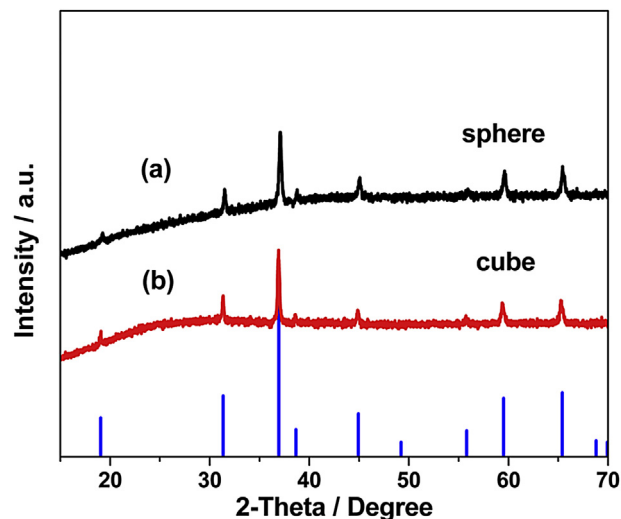

Fig. 1. XRD patterns of (a) s-Co_3O_4 and (b) c-Co_3O_4 materials.

obtained slurry was pasted on Cu foil using the doctor blade technique and dried in a vacuum oven at 120 °C overnight. The electrode disk with the diameter of 12 mm had approximately 3 mg cm^{-2} of active material, which was exactly weighed. The coincell consisted of a working electrode and a lithium foil which was separated by a Celgard 2400 membrane was assembled in an argon filled glove box under the condition without oxygen and water. The electrolyte solution was prepared by dissolving 1 M of $LiPF_6$ in a mixed solvent of ethylene carbonate and diethyl carbonate with a weighing ratio of 1:1 as the electrolyte. Galvanostatic charge−discharge tests were performed by using a battery testing system (LAND CT 2001 A) in the voltage range between 0.01 and 3 V. The cyclic voltammetry (CV) measurements were performed using a VMP3 Electrochemical workstation (Bio-logic Inc) at a scanning rate of 0.1 mV s^{-1}.

3. Results and discussion

Fig. 1 shows the XRD patterns of the Co_3O_4 samples with different morphologies. Fig. 1(a) and (b) corresponds to the calcined Co_3O_4 spheres and cubes, respectively. Both of the XRD patterns agree well with standard Co_3O_4 (JCPDS card: 74-1657). No peaks of impurities are detected, revealing the high purity of the Co_3O_4 materials.

SEM and HRTEM images of different kinds of Co_3O_4 with micro/nano-structure are presented in Fig. 2. Fig. 2(a)−(c) displays SEM images of s-Co_3O_4 obtained under different magnifications and Fig. 2(e)−(g) displays SEM images of c-Co_3O_4 observed under different magnifications, respectively. The micro-particle size of the s-Co_3O_4 in Fig. 2(a) and (b) is estimated to be 2 μm and the size of the s-Co_3O_4 nano-particle in Fig. 2(c) is about 100 nm. As shown in Fig. 2(e)−(g), the size of the c-Co_3O_4 is around 2 μm and the nano-particle size of the c-Co_3O_4 is also around 100 nm. The HRTEM images in Fig. 2(d) and (h) shows the lattice planes of the spheres and cubes morphology, respectively. As can be seen, the lattice planes of s-Co_3O_4 and c-Co_3O_4 are well resolute. From the lattice fringes of Fig. 2(d), the interplanar spacing (*d*-value) is estimated to be 4.681 Å, which matches well with the interplanar distance of the (1 1 1) plane obtained from the XRD pattern of s-Co_3O_4. From Fig. 2(h), the interplanar spacing is 4.671 Å, which is also consistent well with that of the (1 1 1) plane obtained from the XRD pattern of c-Co_3O_4.
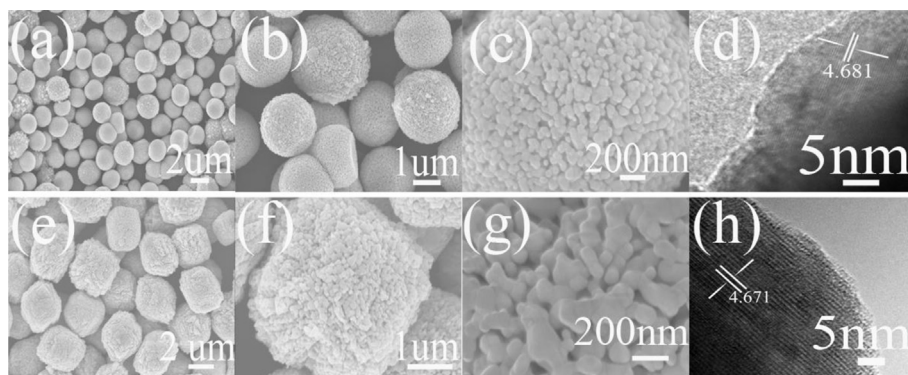
Fig. 2. Typical SEM and HR-TEM images of (a)–(d) s-Co_3O_4 and (e)–(h) c-Co_3O_4 materials.

Fig. 3(a) shows the nitrogen adsorption and desorption isotherms of Co_3O_4 materials with different morphology. The two isotherms are similar to each other in form and can be classified as type IV isotherm according to the IUPAC [14]. In the medium relative pressure region, the adsorption of N_2 increases steadily with the increase of relative pressure due to the capillary condensation and multilayer adsorption in the meso-pores. The sharp climbing in the high pressure region can be attributed to the adsorption in the voids among nanoparticles. The Brunauer–Emmett–Teller (BET) surface areas of the two materials are determined to be 10.774 and 7.0293 $m^2\,g^{-1}$. The pore size distributions of the two Co_3O_4 materials calculated by BJH method are shown in Fig. 3(b). It can be seen that the pore size is in the range of 40–82 nm for s-Co_3O_4 and 40–83 nm for c-Co_3O_4, but the pore size of c-

Co_3O_4 is more uniform than that of s-Co_3O_4. The result is confirmed further by the mercury porosimetry, which is shown in Fig. 3(c). It can be seen that the pore size are both 77 nm for the two materials, and the pore size of c-Co_3O_4 is exactly more uniform than that of s-Co_3O_4. The two methods get the similar results. The void space (pore volume) of the two materials which are obtained based on the nitrogen adsorption–desorption isotherms are 0.128 $cm^3\,g^{-1}$ for s-Co_3O_4 and 0.088 $cm^3\,g^{-1}$ for c-Co_3O_4, respectively. It is obvious to note that the void space of s-Co_3O_4 is larger than that of c-Co_3O_4

Fig. 4 illustrates the cyclic voltammograms of the two Co_3O_4 electrodes at the scanning rate of 0.1 mV s^{-1}. As shown in Fig. 4(a), in the first cycle, the appearance of shoulder at around 1.07 V (A) for s-Co_3O_4 (1.09 V (A′) for c-Co_3O_4) could be attributed to the reduction of Co_3O_4 into CoO and Li_2O. The cathodic peak at 0.87 V for s-Co_3O_4 (0.90 V for c-Co_3O_4) can be attributed to the further reduction of CoO into Co and Li_2O as well as the irreversible formation of a SEI layer [15]. The anodic peak at 2.07 V for s-Co_3O_4 (2.05 V for c-Co_3O_4) can be ascribed to the reversible oxidation of Co to cobalt oxide. In the following cycles, the cathodic peak shifts to 1.14 V for s-Co_3O_4 (1.15 V for c-Co_3O_4) and the anodic peak shifts to 2.12 V for s-Co_3O_4 (2.05 V for c-Co_3O_4). Moreover, the two as-prepared Co_3O_4 electrodes have similar trend in the following cycles indicating a good cyclic performance during the lithiation/delithiation processes. It is worth to mention that a very weak cathodic peak appears at 2.13 V (B) instead of the shoulder at 1.07 V after the first cycle for s-Co_3O_4 (a very weak cathodic peak appears at 2.15 V (B′) instead of the shoulder at 1.09 V after the first cycle for c-Co_3O_4), which can be explained by the much smaller size of the reacting grains after one cycle than in the initial oxides and the size of the clusters is not affected by extensive cycling, at least for a few cycles [16,17].

The electrochemical performances of the two kinds of Co_3O_4 with micro/nano-structure are evaluated by galvanostatic discharge/charge cycling at a current density of 60 mA g^{-1} in Fig. 5. Fig 5(a) and (b) shows the discharge/charge profiles of the s-Co_3O_4 and c-Co_3O_4 electrodes in the 1st, 2nd, 10th, 20th and 25th cycles. Both of them show a short voltage plateau at 1.22 V, which is confirmed by the shoulder at A (A′) point in Fig. 4; and a long voltage plateau at 1.17 V corresponding to the cathodic peak at 0.87 V (0.90 V) in Fig. 4, followed by a sloping curve down to the cutoff voltage of 0.01 V, indicates the typical characteristics of voltage trends for the Co_3O_4 anode [18]. The first discharge and charge capacities are 1323.2 and 976.9 mAh g^{-1} for s-Co_3O_4 electrode, and 961.6 and 711.5 mAh g^{-1} for c-Co_3O_4 electrode, respectively. The capacities of the both electrodes are larger than their theoretical values (890 mAh g^{-1}). This is usually attributed to the boundary area of the nanosized Co_3O_4 with micro/nano-structure,
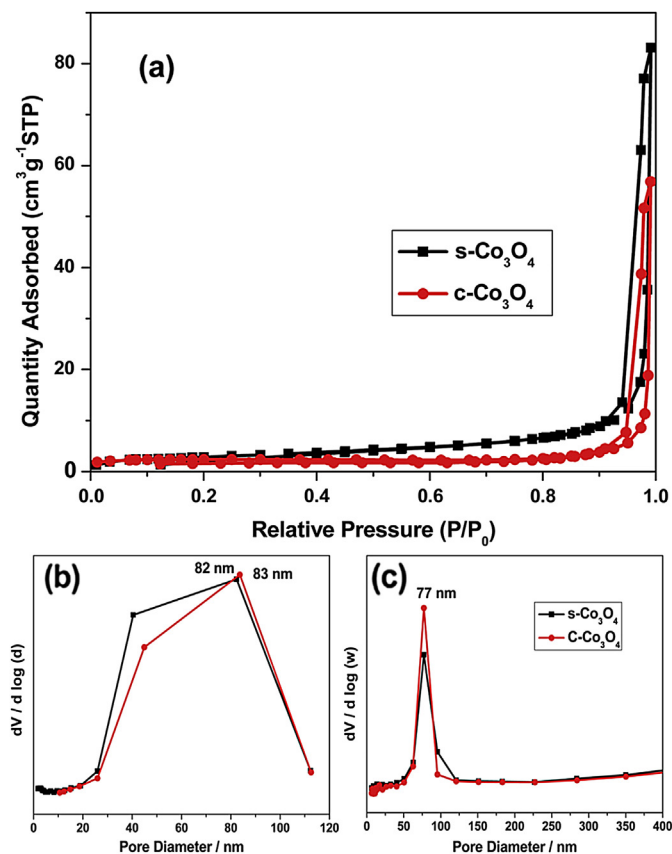

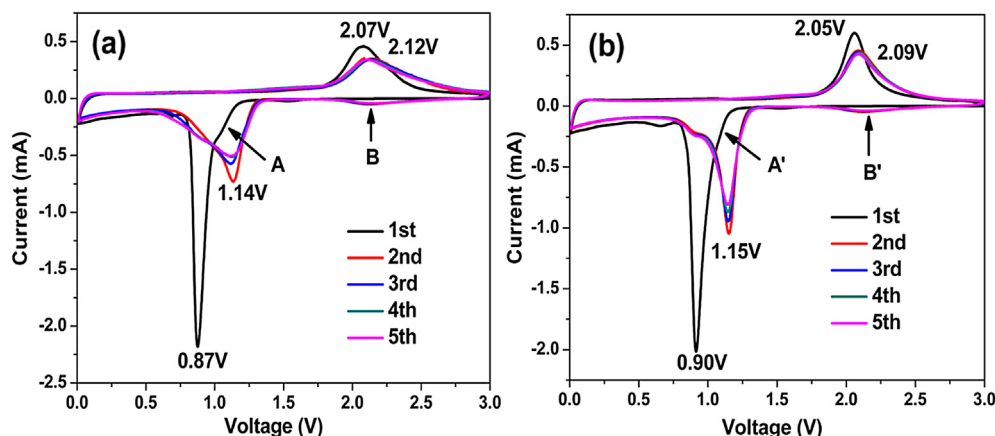**Fig. 3.** Nitrogen adsorption–desorption isotherms for s-Co_3O_4 and c-Co_3O_4 materials.

Fig. 4. Cyclic voltammograms of (a) s-Co_3O_4 and (b) c-Co_3O_4 electrodes at the scanning rate of 0.1 mV s^{-1}.

irreversible reactions to form a solid electrolyte interphase (SEI) layer and possibly interfacial lithium storage [19]. After the first cycle, both of the Co_3O_4 electrodes exhibit excellent electrochemical lithium storage performance. Surprisingly, after 10 discharge/charge cycles, they exhibit a high reversible capacity of 1152.7 and 1131.4 mAh g^{-1} for s-Co_3O_4 electrode, 772.3 and 756.6 mAh g^{-1} for c-Co_3O_4 electrode, respectively. The corresponding coulombic efficiencies rise rapidly from 73.8% to 74.0% in the first cycle to 98.2% and 98.0% in the 10th cycle and then remain constant in the following cycles. More importantly, the reversible capacities of the both Co_3O_4 electrodes increase slightly with cycling and the discharge capacities reach ∼1290.2 and 792.6 mAh g^{-1} after 25 cycles, and they present a much better cycling performance than the results as previously reported [20].

The charge capacities exceed the theoretical value, indicating that the excess capacity is associated with increased charge storage within the polymeric surface layer. When the Co_3O_4 electrode is fully reduced by lithium, some 10−20 Å metallic nanoparticles will be shown [21]. Therefore, the metallic nanoparticles are dispersed in a lithia matrix, and the mixture is surrounded by a solid electrolyte interface to form a new "composites". The nano-sized and pseudo-amorphous characters of the composite electrode, once created during the first discharge of the composite electrode, are preserved on the following charge. Partial of the "composites" grows/disappears in the subsequent cycles, according to Sun's research about the growth/disappearance of the SEI layer [22]. As the charge of the half-cell, partial "composites" disappears and the extra lithium would be released from the "composites", so the

charge capacity can exceed the theoretical value. With the cycling process, the "composites" becomes larger. The nanoparticles conglomerate with each other by the "composites", which is further confirmed by Fig. 6. Fig. 6 shows the TEM images of s-Co_3O_4 electrodes after different cycles. From (a) to (c), the thickness of the "composites" is 4.2, 9.27 and 50.83 nm, respectively. Especially, after 140 cycles at the current density of 400 mA g^{-1} (Fig. 6(b)), the s-Co_3O_4 electrode is coated by an obvious "composites" layer. Meanwhile, the electrode nanoparticle break in many smaller particles. So, we think the increase of volume is not because of the extendability of the particle, but because of the existence of the "composites".

To further evaluate the electrochemical properties of the two Co_3O_4 electrodes, galvanostatic discharge/charge reactions are performed at the current densities of 400 and 1000 mA g^{-1} in Fig. 7. Fig. 7(a) shows the cycling performance of the two Co_3O_4 electrodes at the current density of 400 mA g^{-1}. In the first 20 cycles (except for the 1st discharge), the capacities increase slightly and then reach to 1093 mAh g^{-1} for s-Co_3O_4 and 750.2 mAh g^{-1} for c-Co_3O_4, respectively. The discharge capacity can be maintained after 70 cycles and decrease slightly to 970 mAh g^{-1} after 140 cycles for s-Co_3O_4 electrode. Meantime, for the c-Co_3O_4 electrode, the discharge capacity decrease slightly to 490 mAh g^{-1} after 140 cycles.

The superior reversible capacity can be attributed to a variety of favorable reasons. First, ^7Li NMR has been used to explain the higher capacity of hard carbon [23], which may be used to explain the extra capacity of Co_3O_4 electrode, the quasimetallic Li forming a
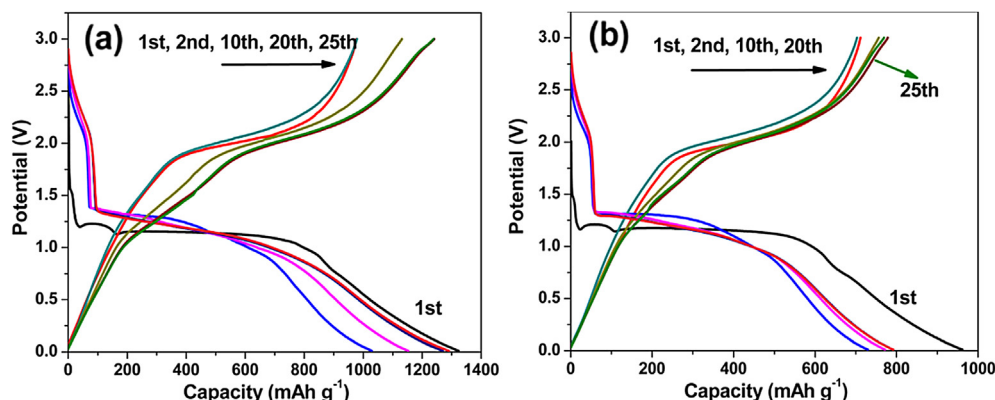

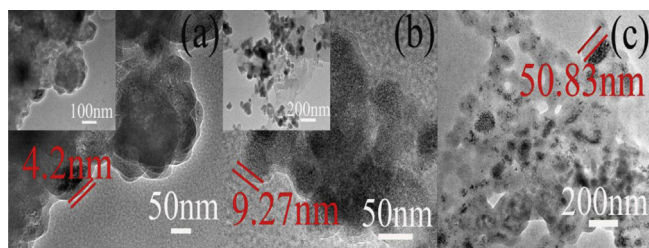**Fig. 5.** Discharge/charge curves of (a) s-Co_3O_4 and (b) c-Co_3O_4 electrodes at the current density of 60 mA g^{-1}.

Fig. 6. TEM images of s-Co_3O_4 electrode: (a) 60 mA g^{-1} after 25 cycles, (b) 400 mA g^{-1} after 140 cycles and (c) 1000 mA g^{-1} after 500 cycles.

lithium cluster in the pore of the micro/nano-structure Co_3O_4. Second, some of the extra reversible capacity may be attributed to the absence of the AB (see Fig. S1 in the ESI).

Fig. 7(b) illustrates the cycling performance of the two Co_3O_4 electrodes at the current density of 1000 mA g^{-1}. The capacities of the both electrodes decrease greatly in the first several cycles, however, after 100 cycles, the capacity of s-Co_3O_4 electrode can retain almost the same value until the 500 cycles and the capacity of c-Co_3O_4 decreases slowly until the 500 cycles. After 500 cycles, the discharge capacity of s-Co_3O_4 is still 500 mAh g^{-1} but that of the c-Co_3O_4 is only 257 mAh g^{-1}

Fig. 8 illustrates the rate performance of the s-Co_3O_4 and c-Co_3O_4 electrodes at different current densities (60 mA g^{-1}, 0.5, 1, 2, 5 and 10 A g^{-1}) for every ten cycles. With increasing current density, the capacities of the two Co_3O_4 electrodes decrease monotonically. Both of them exhibit the excellent rate performance, even at the current density 2 A g^{-1}, the capacity is still 450 mAh g^{-1} for s-Co_3O_4 electrode and 406 mAh g^{-1} for c-Co_3O_4 electrode. When the current density return to 0.5 A g^{-1}, the value of capacity is able to recover to about 820 mAh g^{-1} for s-Co_3O_4 electrode and 613 mAh g^{-1} for c-Co_3O_4 electrode. Both of them are close to the capacity of 0.5 A g^{-1} at the first time. However, it can be clearly
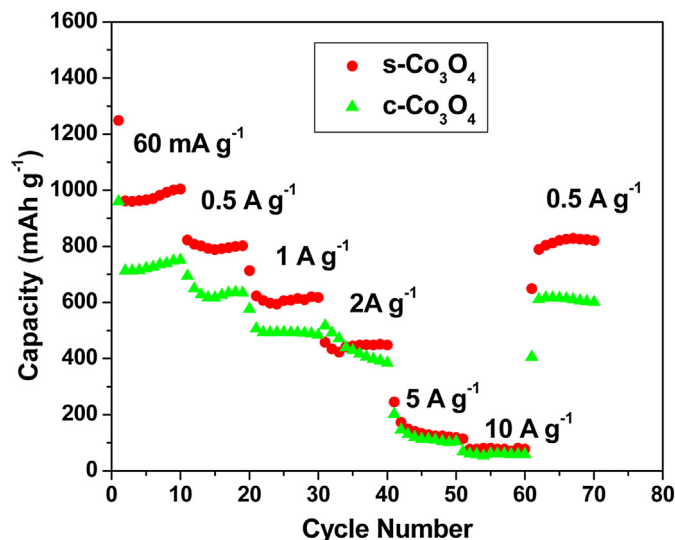

Fig. 8. Rate performances of s-Co_3O_4 and c-Co_3O_4 electrodes at the current densities of 60 mA g^{-1}, 0.5, 1, 2, 5 and 10 A g^{-1} for ten cycles at every current density.

observed that the rate capability of s-Co_3O_4 is much better than that of c-Co_3O_4.

It is obvious to note that the electrochemical performance of the s-Co_3O_4 electrode is better than that of c-Co_3O_4 electrode, which can be attributed to the BET surface, pore size, volume and pore distribution. First, the higher BET surface of s-Co_3O_4 can provide more active reaction sites, thereby increasing the capacity of the electrode; second, the larger volume, the same pore size and the less uniform pore distribution mean the larger amount of pores, which enhance the electrolyte/Co_3O_4 contact area, shorten the Li$^+$ ion diffusion length and accommodate the mechanical strain; third, the larger void volume provides more space for the expanded of the
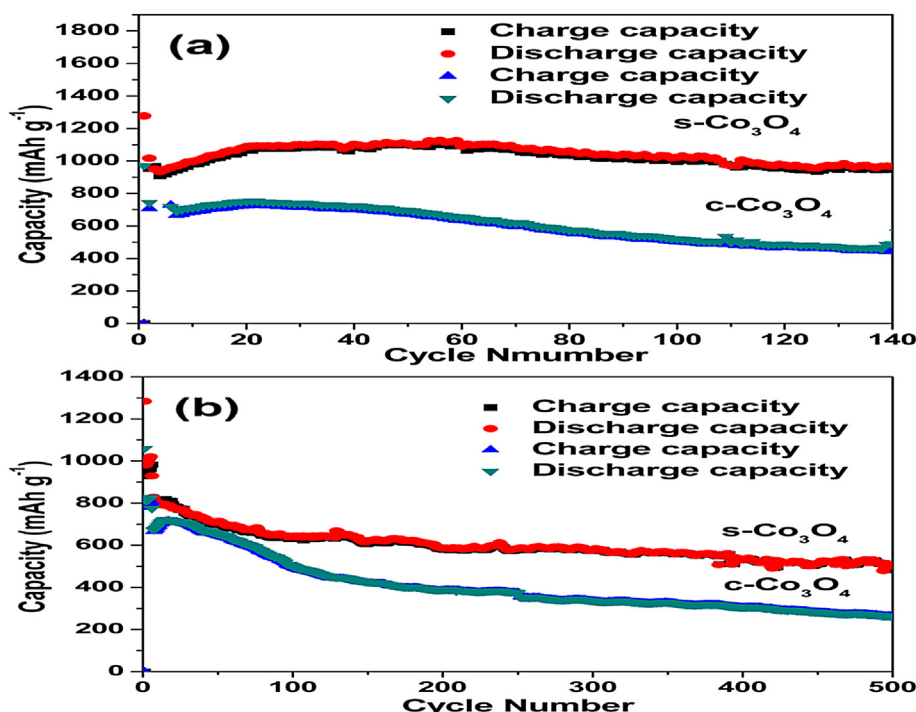

Fig. 7. Cycling performances of the two Co_3O_4 electrodes at the current density of (a) 400 mA g^{-1} and (b) 1000 mA g^{-1}.
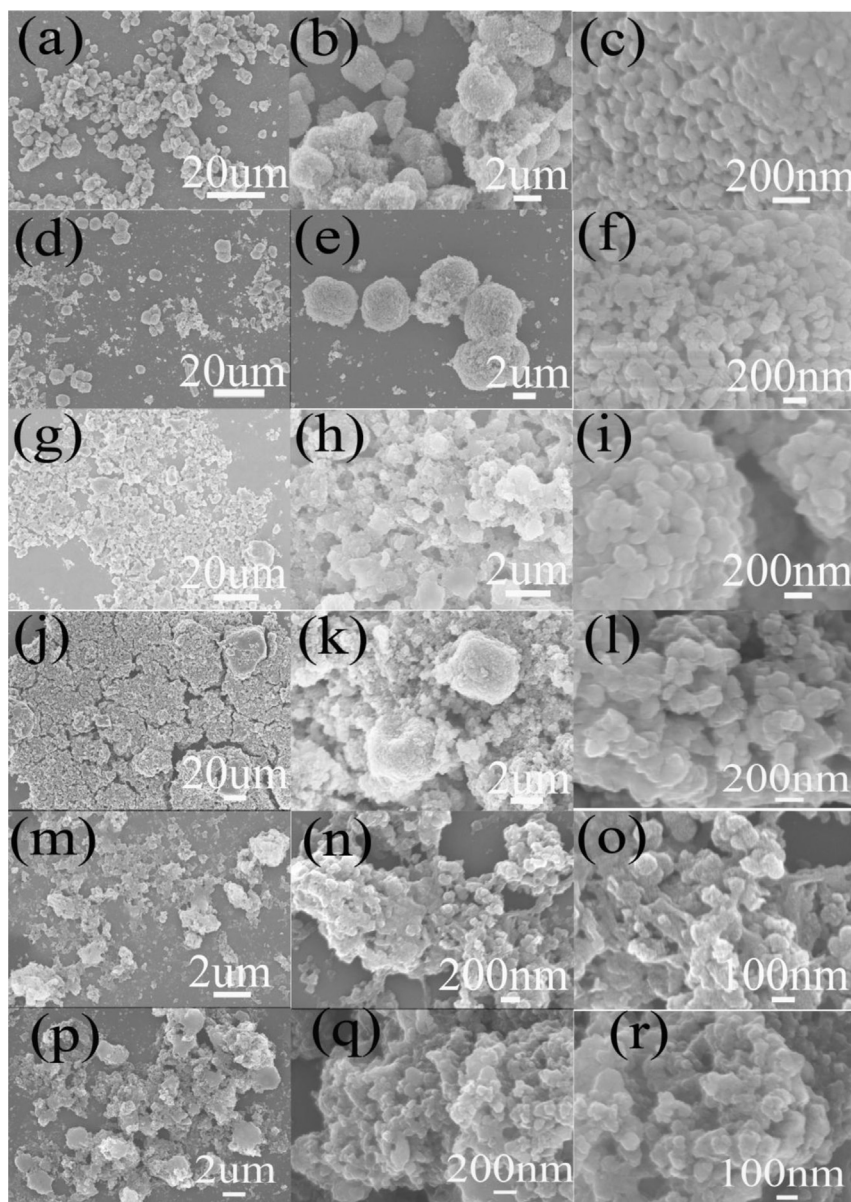
Fig. 9. SEM images of Co_3O_4 electrodes: (a)–(c) 60 mA g^{-1} after 25 cycles, (g)–(i) 400 mA g^{-1} after 140 cycles and (m)–(o) 1000 mA g^{-1} after 500 cycles for s-Co_3O_4; (d)–(f) 60 mA g^{-1} after 25 cycles, (j)–(l) 400 mA g^{-1} after 140 cycles and (p)–(r) 1000 mA g^{-1} after 500 cycles for c-Co_3O_4.

Co_3O_4 particles as the cycling of charge/discharge progress, thus leading to a larger contact surface with the electrolyte as well as better structure stability.

To further confirm the reason of the discrepancy between the s-Co_3O_4 and c-Co_3O_4 electrodes, SEM and TEM characterizations are employed. Fig. 9 displays the SEM images of the two Co_3O_4 materials which are fully charged after different cycles. Fig. 9(a)–(c) and (d)–(f) is presented after 25 cycles at the current density of 60 mA g^{-1}. It can be clearly seen that the shape of two materials can be maintained. The size of spheres and cubes are still around 2 μm and the nanoparticles are still around 100 nm. There are no obvious changes to the starting Co_3O_4 materials shown in Fig. 2. Fig. 9(g)–(i) and (k)–(l) shows the morphology of the two electrodes after 140 cycles at the current density of 400 mA g^{-1}. The shape of spheres and cubes are partly destroyed and the void space of the two electrodes disappears because of the expansion of the nanoparticles after Li insertion. However, the nanoparticles from the spheres are able to keep the morphology but some of the

nanoparticles from the cubes broke up into smaller particles. The collapse of the nanoparticles will lead to electric isolation, resulting in capacity fading. Note that the capacity for s-Co_3O_4 decreases slowly than that of c-Co_3O_4, which may benefit from the morphology maintenance of the nanoparticles [24]. Fig. 9(m)–(o) and (p)–(r) shows the two electrodes after 500 cycles at the current density of 1000 mA g^{-1}. Both the shape of spheres and cubes destroyed completely and the nanoparticles agglomerate with each other. So, the capacity of Co_3O_4 decreases pronouncedly.

4. Conclusion

Two kinds of Co_3O_4 materials with micro/nano-structure are successfully synthesized in a facile route. The Co_3O_4 electrode with micro/nano-structure combines the advantages of the micro-structure and nano-structure. Both of the s-Co_3O_4 and c-Co_3O_4 electrodes have the good rate capacity and superior cyclic stability resulted from the small diffusion lengths in the nanoparticles and

few side reactions with the electrolyte for the microparticles. However, the performance of the s-Co_3O_4 electrode is much better than that of the c-Co_3O_4 electrode because of the larger void space. The reversible capacity of s-Co_3O_4 electrode can still reach 970 mAh g^{-1} after 140 cycles at a current density of 400 mA g^{-1} and 500 mAh g^{-1} after 500 cycles at a current density of 1000 mA g^{-1}, which is much higher than the previously reported results. Therefore, we conclude that the micro/nano-structure is very important for the electrodes, meaning that we are able to design and synthesize electrode materials with appropriate structure to improve the electrochemical performance.

Acknowledgments

Appendix A. Supplementary data

Supplementary data related to this article can be found at http://dx.doi.org/10.1016/j.jpowsour.2013.09.074.

References

[1] J. Chen, F. Cheng, Acc. Chem. Res. 42 (2009) 713—723.
[2] Y. Li, B. Tan, Y. Wu, Nano Lett. 8 (2007) 265—270.
[3] N.A. Kaskhedikar, J. Maier, Adv. Mater. 21 (2009) 2664—2680.
[4] P. Meduri, C. Pendyala, V. Kumar, G.U. Sumanasekera, M.K. Sunkara, Nano Lett. 9 (2009) 612—616.
[5] Y.S. Hu, L. Kienle, Y.G. Guo, J. Maier, Adv. Mater. 18 (2006) 1421—1426.
[6] C. Wu, P. Yin, X. Zhu, C. OuYang, Y. Xie, J. Phys. Chem. B 110 (2006) 17806—17812.
[7] W. Yao, J. Yang, J. Wang, Y. Nuli, J. Electrochem. Soc. 155 (2008) A903—A908.
[8] J.W. Seo, J.T. Jang, S.W. Park, C. Kim, B. Park, J. Cheon, Adv. Mater. 20 (2008) 4269—4273.
[9] J.L.C. Rowsell, V. Pralong, L.F. Nazar, J. Am. Chem. Soc. 123 (2001) 8598—8599.
[10] P. Novák, K. Müller, K.S.V. Santhanam, O. Haas, Chem. Rev. 97 (1997) 207—282.
[11] A.S. Arico, P. Bruce, B. Scrosati, J.M. Tarascon, W. van Schalkwijk, Nat. Mater. 4 (2005) 366—377.
[12] J. Chen, X.H. Xia, J.P. Tu, Q.Q. Xiong, Y.X. Yu, X.L. Wang, C.D. Gu, J. Mater. Chem. 22 (2012) 15056—15061.
[13] P.G. Bruce, B. Scrosati, J.M. Tarascon, Angew. Chem. Int. Ed. 47 (2008) 2930—2946.
[14] K.S.W. Sing, D.H. Everett, R.A.W. Haul, L. Moscou, R.A. Pierotti, J. Rouquerol, T. Siemieniewska, Pure Appl. Chem. 57 (1985) 603—619.
[15] S. Laruelle, S. Grugeon, P. Poizot, M. Dollé, L. Dupont, J.-M. Tarascon, J. Electrochem. Soc. 149 (2002) A627—A634.
[16] D. Larcher, G. Sudant, J.B. Leriche, Y. Chabre, J.M. Tarascon, J. Electrochem. Soc. 149 (2002) A234—A241.
[17] F. Wang, C. Lu, Y. Qin, C. Liang, M. Zhao, S. Yang, Z. Sun, X. Song, J. Power Sources 235 (2013) 67—73.
[18] W.Y. Li, L.N. Xu, J. Chen, Adv. Funct. Mater. 15 (2005) 851—857.
[19] H.-J. Liu, S.-H. Bo, W.-J. Cui, F. Li, C.-X. Wang, Y.-Y. Xia, Electrochim. Acta 53 (2008) 6497—6503.
[20] N. Jayaprakash, W.D. Jones, S.S. Moganty, L.A. Archer, J. Power Sources 200 (2012) 53—58.
[21] P. Poizot, S. Laruelle, S. Grugeon, L. Dupont, J.M. Tarascon, Nature 407 (2000) 496—499.
[22] Z. Yuan, F. Huang, C. Feng, J. Sun, Y. Zhou, Mater. Chem. Phys. 79 (2003) 1—4.
[23] H. Fujimoto, A. Mabuchi, K. Tokumitsu, N. Chinnasamy, T. Kasuh, J. Power Sources 196 (2011) 1365—1370.
[24] X. Wang, X.L. Wu, Y.G. Guo, Y. Zhong, X. Cao, Y. Ma, J. Yao, Adv. Funct. Mater. 20 (2010) 1680—1686.